Chapter 3

BOSE-EINSTEIN CONDENSATE MODEL: AN APPROACH TO GET RID OFF FROM PROBLEMS IN CDM MODELS.

3.1 Introduction

One of the most acceptable way to explain the dark (invisible) matter scenario, distributed in a spherical halo around the galaxies, is the Bose-Einstein Condensation (BEC) model which is, firstly, observed in 1995 by the experiments on vapours of rubidium (Anderson et al., 1995) and sodium (Davis et al., 1995). A dilute atomic Bose gas enclosed in a trap and cooled to very low temperatures is an ideal system for the experimental observation of the Bose-Einstein condensate. Particles in a dilute Bose gas can occupy the same quantum ground state at very low temperature to form Bose-Einstein condensate (BEC) stars. BEC can be found not only in momentum

space but also in coordinate space which is very implacable in both the theoretical and experimental points of view and offers an important models to search the fact like the temperature dependence of the condensation, energy and density distributions, interference phenomena, frequencies of collective excitations and so on.

BEC is a particular case of coherence phenomena in which all the particles are in the same quantum state. Due to the cooling of the gas, the condensation of a large part of the particles in the gas takes place via a phase transition which occurs when the wavelengths of individual particles overlap and behave identically. Strongly correlation among the particles is an important condition for the transition to take place [1, 2]. The momentum distribution of the atoms of helium measured in neutron scattering experiments (Sokol, 1995), paraexcitons in semiconductors (Wolfe, Lin and Snoke, 1995) are few evidences for BEC.

A dilute Bose-Einstein gas with only two-body mean field interaction near zero temperature can be modelled with the Gross-Pitaevskii equation [2]. An analytical equation of the mass-radius relation of a Newtonian self-gravitating Bose-Einstein condensation described by the Gross-Pitaevskii-Poisson system, obtained in [3]. A numerical solution of the hydrostatic equilibrium equation that balances between the gravitational attraction and the pressure due to quantum effects or short-range interactions (scattering), obtained in [4]. The core-cusp problem which is an important problem faced by many standard CDM models can be solved by considering that the dark matter is the composition of ultralight scalar particles, initially in a cold

Bose-Einstein condensate, with masses of the order of 10^{-22} eV [5].

When particles (bosons) have a correlation with each other then the Bose-Einstein condensation occurs. This is possible when their wavelengths overlap i.e. the mean inter-particles distance a is less than the thermal wavelength $\lambda_T = \sqrt{2\pi h^2/mk_BT}$ where T, m and k_B are respectively the thermodynamic equilibrium temperature, particle mass and the Boltzmann's constant [1, 2]. Therefore, the critical temperature for the condensation is given by $T_{cr} < 2\pi h^2 n^{2/3}/mk_B$ where $n = a^{-3}$ is the particle number density.

In CDM paradigm, there are two types of halo models. One is idealized models obtained from a Kinetic Theory approach, it may based on specific theoretical consideration or on convenient ansatzes. The other one is based on universal mass density profiles obtained empirically from the outcomes of N–body numerical simulations [6, 7]. Navarro–Frenk–White model is one such a model that emerge from the latter approach and is based on Navarro-Frenk-White (NFW) [7, 8] numerical simulations. Here, we will discuss important features of both the halo models, BEC and NFW, and a brief comparison between them are mentioned there in.

3.2 Static Newtonian Bose-Einstein Condensate

In case of a static Bose-Einstein condensate where all the physical quantities are independent of time, the governing field equations reduced to [9]

$$\nabla P(\rho_m/m) = -\rho_m \nabla(\frac{V}{m}), \tag{3.1}$$

$$\nabla^2 V = 4\pi G \rho_m, \tag{3.2}$$

where $\rho_m = m\rho$ is the mass density inside the Bose-Einstein condensate, m is the mass of the condensed particles, $P(\rho_m/m) = g^{'}(\rho_m/m)(\rho_m/m) - g(\rho_m/m)$, $g(\rho)$ is an arbitrary non-linear term with $g^{'} = dg/d\rho$ and V is the gravitational potential.

Assume the non-linearity as

$$g(\rho) = \alpha\rho^{\Gamma}, \tag{3.3}$$

where $\alpha > 0$ and $\Gamma > 0$ are constants. The equation of state of the gravitational Bose-Einstein condensate, now, simplifies to,

$$P(\rho_m) = \alpha(\Gamma - 1)\rho_m^{\Gamma} = K\rho_m^{\Gamma} \ , \tag{3.4}$$

which is a polytropic equation where $K = \alpha(\Gamma - 1)$.

Introducing the dimensionless coordinate ξ via $r = [(n+1)K\rho_{cm}^{1/n-1}/4\pi G]^{1/2}\xi$ and taking $\rho_m = \rho_{cm}\theta^n$ where θ is a dimensionless variable and ρ_{cm} is the central density of the condensate [10], the structure of the static gravitationally bounded Bose-Einstein condensate can be expressed as the Lane-Emden equation [9]

$$\frac{1}{\xi^2}\frac{d}{d\xi}(\xi^2\frac{d\theta}{d\xi}) + \theta^n = 0, \tag{3.5}$$

with polytropic index $n = 1/(\Gamma - 1)$.

Defining ξ_1 as the zero-pressure and zero-density surface of the condensate i.e. $\theta(\xi_1) = 0$, the radius and the mass of the condensation can be obtained as

$$R = [\frac{(n+1)\alpha}{4\pi G n}]^{1/2} \rho_{cm}^{(1-n)/2} \xi_1, \tag{3.6}$$

and

$$M = 4\pi [\frac{(n+1)\alpha}{4\pi G n}]^{3/2} \rho_{cm}^{(3-n)/2n} \xi_1^2 \left|\theta'(\xi_1)\right|, \tag{3.7}$$

respectively [9].

In another approach which is considered as one of the standard approach to the Bose-Einstein condensation, one can choose the non-linearity term as

$$g(\rho) = \frac{u_0}{2} |\psi|^4 = \frac{u_0}{2} \rho^2, \tag{3.8}$$

where $u_0 = 4\pi\hbar^2 a/m$, a is the inter-particle scattering length [1]. Then the equation of state of the condensate is given by

$$P(\rho_m) = U_0 \rho_m^2, \tag{3.9}$$

which is a polytropic equation with index $n = 1$, where

$$U_0 = 2\pi\hbar^2 a/m^3. \tag{3.10}$$

The solution of the Lane-Emden Eq.(3.5) for the present case can be obtained as

$$\theta(\xi) = \frac{\sin \xi}{\xi}, \tag{3.11}$$

which satisfies the boundary condition $\theta(0) = 1$ [10].

The radius of the gravitationally bound system is defined by the condition $\theta(\xi_1) = 0$ which corresponds to $\xi_1 = \pi$. Then the radius R of the Bose-Einstein condensate is [9]

$$R = \pi\sqrt{\hbar^2 a/Gm^3}, \tag{3.12}$$

which is independent of the central density but the total mass of the condensate

$$M = 4\pi^3(\hbar^2 a/Gm^3)^{3/2}\rho_{cm}\left|\theta^{'}(\xi_1)\right| = 4\pi^2(\hbar^2 a/Gm^3)^{3/2}\rho_{cm} = \frac{4R^3\rho_{cm}}{\pi}, \tag{3.13}$$

where $\left|\theta^{'}(\xi_1)\right| = 1/\pi$ is not. With the help of the Eq.(3.13), the mean density of the condensate $\langle\rho_m\rangle$ simplifies to

$$\begin{aligned}\langle\rho_m\rangle &= \frac{3M}{4\pi R^3} \\ &= 3\rho_{cm}/\pi^2.\end{aligned} \tag{3.14}$$

3.3 Dark Matter as a Bose-Einstein Condensate

From Eq.(3.11), it follows that if the dark matter is formed due to Bose-Einstein condensation, it's density distribution would be [9]

$$\rho_{\rm DM}(r) = \rho_{\rm DM}^{(c)}\frac{\sin kr}{kr}, \tag{3.15}$$

where $k = \sqrt{\frac{Gm^3}{\hbar^2 a}}$ and $\rho_{\rm DM}^{(c)}$ is the central density of the condensate i.e. $\rho_{DM}^{c} = \rho_{DM}(0)$.

Corresponding mass profile is given by

$$\begin{aligned} m_{\rm DM}(r) &= \int_0^r 4\pi\rho_{\rm DM}(r)r^2dr \\ &= (\frac{4\pi\rho_{\rm DM}^{(c)}}{k^2}r)(\frac{\sin(kr)}{kr}-\cos(kr)). \end{aligned} \tag{3.16}$$

Therefore, the tangential velocity of a test particle moving in this halo is given by

$$\begin{aligned} v_{tg}^2(r) &= Gm_{\rm DM}(r)/r \\ &= \frac{4\pi\rho_{\rm DM}^{(c)}G}{k^2}(\frac{\sin(kr)}{kr}-\cos(kr)). \end{aligned} \tag{3.17}$$

The boundary of the halo is defined by the radius $R_{\rm DM}$ for which the density of the Bose-Einstein condensate is negligible i.e. $\rho_{\rm DM}(R_{\rm DM}) = 0$ giving $R_{\rm DM} = \frac{\pi}{k}$. Therefore, the radius and total mass of the dark matter condensate are, respectively, as follows

$$R_{\rm DM} = \pi\sqrt{\frac{\hbar^2 a}{Gm^3}}, \tag{3.18}$$

$$M_{\rm DM} = m_{\rm DM}(R_{\rm DM}) = \frac{4R_{\rm DM}^3\rho_{\rm DM}^{(c)}}{\pi}. \tag{3.19}$$

Tangential velocity of a test particle near the vacuum boundary can be obtained from Eq.(3.17) as

$$v_{tg}^2(R_{\rm DM}) = \frac{4\pi\rho_{\rm DM}^{(c)}G}{k^2} = \frac{4\rho_{\rm DM}^{(c)}GR_{\rm DM}^2}{\pi}, \tag{3.20}$$

which is constant for a particular galaxy.

A complete study on the Eqs.$(3.15-3.20)$ can unveil the physical properties of the galactic dark matter condensates and these equations together with Eqs.(3.12) and (3.13) can constrain on the physical properties of the condensate namely on the

central dark matter density of the condensate, $\rho_{\rm DM}^{(c)}$, and on the dark matter radius, $R_{\rm DM}$, which are very essential for the stability of the dark matter halo structure.

A restriction on the maximum central density of the Bose-Einstein condensate star due to the quadric nonlinearity and with equation of state $P(\rho) = U_0\rho^2$, can be found from the causality condition $c_s < c$ where c is the speed of light and c_s is that of the sound given by $c_s^2 = \frac{\partial P}{\partial \rho}$. The causality condition gives [11]

$$\rho_{\rm DM}^{(c)} \leq \frac{m^3c^2}{4\pi a\hbar^2} = 2.42 \times 10^{16}\kappa^{-2}\ {\rm g/cm^3} \rightarrow 2.42 \times 10^{16}\ {\rm g/cm^3}, \tag{3.21}$$

for $a = 1$fm and $m = 2m_n$, where

$$\kappa = (\frac{a}{1\ {\rm fm}})^{1/2}(\frac{m}{2m_n})^{-3/2}, \tag{3.22}$$

and $m_n = 1.6749 \times 10^{-24}$g is the mass of the neutron.

With the help of Eq.(3.21), restriction on the maximum mass of the Bose-Einstein condensate star can be obtained from Eq.(3.19) as [11]

$$M = \frac{4R_{\rm DM}^3\rho_{\rm DM}^{(c)}}{\pi} \leq \frac{\pi c^2\hbar\sqrt{a}}{(Gm)^{3/2}} = 4.46\kappa M_\odot \rightarrow 4.46M_\odot, \tag{3.23}$$

for $a = 1$fm and $m = 2m_n$.

A stronger limit on both the mass and central density can be found from the condition that the radius $R_{\rm DM}$ of the Bose-Einstein condensate star must be greater than the Schwarzschild radius $R_S = \frac{2GM}{c^2} = \frac{8GR_{\rm DM}^3\rho_{\rm DM}^{(c)}}{\pi c^2}$ i.e. $R_{\rm DM} \geq R_S$. This will govern to [11]

$$\rho_{\rm DM}^{(c)} \leq \frac{m^3c^2}{8\pi a\hbar^2} = 1.21 \times 10^{16}\ \kappa^{-2}\ {\rm g/cm^3} \rightarrow 1.21 \times 10^{16}\ {\rm g/cm^3}, \tag{3.24}$$

$$M \leq \frac{c^2\hbar\sqrt{a}}{(Gm)^{3/2}}\frac{\pi}{2} = 2.23\kappa M_\odot \rightarrow 2.23 M_\odot. \tag{3.25}$$

The maximum mass of the condensation M_{max}, the maximum central density $(\rho_{\rm DM}^{(c)})_{max}$ and the radius of a dark matter halo ($R_{\rm DM}$) are the functions of the boson mass m and scattering length a (which can be determined by fundamental physics) and κ is proportional to the ratio a/m^3. The general relativistic effect and the best available data for the values of m and a, may lead to a better constrains on the physical parameter of the galactic halo, one such is given by Tolman-Oppenheimer-Volkoff (TOV) [12],

$$\begin{aligned}
(R_{\rm DM})_{\rm min} &= 3.974\kappa \text{ km} \rightarrow 3.974 \text{ km}, \\
M_{\rm max} &= 0.710\kappa M_\odot \rightarrow 0.710 M_\odot, \\
(\rho_{\rm DM}^{(c)})_{\rm max} &= 2.035\times 10^{16}\ \kappa^{-2}\ \text{g/cm}^3 \rightarrow 1.21\times 10^{16}\ \text{g/cm}^3,
\end{aligned} \tag{3.26}$$

($a = 1$fm and $m = 2m_n$).

On the other hand the mass of the particle in the condensate can be obtained from Eq.(3.12), which is

$$m = (\frac{\pi^2\hbar^2 a}{GR^2})^{1/3} \approx 6.73\times 10^{-2}[a(\text{fm})]^{1/3}[R(\text{kpc})]^{-2/3}\ \text{eV}. \tag{3.27}$$

For $a \approx 1$ fm and $R \approx 10$ kpc, the typical mass of the condensate particle (given by Eq.(3.27)) is $m \approx 14$ MeV and that for $a \approx 10^6$ fm is $m \approx 1.44$ eV. These results have a great agreement with the limit $m < 1.87$ eV obtained from cosmological considerations [13].

3.4 Navarro–Frenk–White (NFW) model

The density profile predicts by the Navarro-Frenk-White model [6] can be taken as

$$\rho_{NFW}(r) = \frac{\rho_s}{\frac{r}{r_s}(1+\frac{r}{r_s})^2}, \tag{3.28}$$

where r_s is a scale radius, $\rho_s = \delta_0 \rho_0$ with

$$\rho_0 = \rho_{crit}\Omega_0 h^2 = 253.8\Omega_0 h^2 \frac{M_\odot}{\mathrm{kpc}^3}, \tag{3.29}$$

$$\delta_0 = \frac{\Delta c_0^3}{3[\ln(1+c_0) - \frac{c_0}{1+c_0}]}, \tag{3.30}$$

where the concentration parameter c_0 is given in terms of virial mass M_{vir} [14] by

$$c_0 = 62.1 \times (\frac{hM_{vir}}{M_\odot})^{-0.06}(1+\epsilon), \tag{3.31}$$

and $-1/3 \lesssim \epsilon \lesssim 1/2$, $\rho_{crit} \equiv \frac{3H_0^2}{8\pi} = 1.88 \times 10^{-29}\ h^2$ g/cm^3 is the critical density of the universe.

The virial radius r_{vir} is defined by the condition that the average halo density is Δ times the cosmological one, ρ_0, and can be found from

$$\Delta\rho_0 = \frac{3M_{vir}}{4\pi r_{vir}^3}. \tag{3.32}$$

The factor Δ depends on the chosen model. For a ΛCDM model with $\Omega_0 = 1$, $\Delta \sim 100$ [15].

The mass function in this profile is given by

$$\begin{aligned} M_{NFW}(r) &= \int 4\pi\rho r^2 dr \\ &= 4\pi r_s^3 \rho_s [\ln(1+\frac{r}{r_s}) - \frac{\frac{r}{r_s}}{1+\frac{r}{r_s}}]. \end{aligned} \tag{3.33}$$

The tangential velocity, v_{tg}^{NFW}, that can be obtained by equating the gravitational force with the centrifugal one, is given by

$$v_{tg}^{NFW}(r) = \sqrt{v_0^2(\frac{\ln(1+\frac{r}{r_s})}{\frac{r}{r_s}} - \frac{1}{1+\frac{r}{r_s}})}, \tag{3.34}$$

and the gravitational potential is given by

$$\Phi_{NFW}(r) = -v_0^2 \frac{\ln(1+\frac{r}{r_s})}{\frac{r}{r_s}}, \tag{3.35}$$

where $v_0^2 = 4\pi G r_s^2 \rho_s$ is three times the tangential velocity of particles at the limb of a sphere of radius r_s. It can be mentioned that though $\rho_{NFW}(r)$ diverges at the centre of the halo, other quantities (i.e. M_{NFW}, v_{tg}^{NFW} and Φ_{NFW}) are regular as $r \to 0$. The divergence of $\rho_{NFW}(r)$ at the centre can be remove by replacing a small central region of the NFW halo with an interior Schwarzschild solution with constant density [16].

3.5 Comparison of the BEC model with CDM model

Observations on the high-resolution rotational curves are the evidence for the profound nature of the density profile, presents a nearly constant density core, which is significantly different from the one which is defined by Eq.(3.28) [17]. Observations on the dwarf galaxies (a cosmic structure dominated by dark matter) done by "The HI Nearby Galaxy Survey" (THINGS) [18], showed some worthy discrepancies between observations and simulations done in the scenario of the CDM model. The observations on the rotational curves of the dwarf galaxies show that it rises too slowly

compared to that of the cuspy like dark matter distribution in CDM halos. The mean value of the logarithmic slopes of the mass density profiles of the dwarf galaxies is $\alpha(r) = -0.29 \pm 0.07$ [19] while that for the LSB galaxies is $\alpha(r) = -0.2 \pm 0.2$ [20] which are remarkably different from $\alpha(r) = -1.0$, obtained from dark-matter-only simulations. The luminosity of the dwarf galaxies formed in current hydrodynamical simulations are not the same that we usually expect [21]. This produce a serious problem related to the mass and observed properties of the dwarf galaxies.

Dark matter with ultralight scalar particle having mass of the order of 10^{-22} eV, initially in a cold Bose-Einstein condensate, may be a viable alternative to standard CDM models [5]. A sound agreement between the theoretical predictions and observations of the rotational curves in the BEC model for several High Surface Brightness (HSB), Low Surface Brightness (LSB) and dwarf galaxies, are found in [9]. The following reasons prompt us for the further analysis of the rotational curves :

i. Updated data that are available due to modern telescope system and instruments, may increase the accuracy of rotational curve data for dwarf galaxies which are supposed to be filled with dark matter [18, 19].

ii. It is important to analyze the observed mean values of the logarithmic inner density and velocity slopes to discriminate between different dark matter models. The analysis of the discrepancies, via logarithmic slope, between observations and the theoretical predictions of the CDM models will be more fruitful than the rotational velocity curves analysis.

iii. A directive comparison between the predictions of the density profile (3.28) and that of the BEC profiles may unveil some important features of both the models.

BEC model gives a very good description of the rotational curves for all most all the curves described in [22] where as the NFW velocity fit fails to produce any significant description of the rotational curves, either in the inner region or outer one [22]. At the center of the galaxy, the density profile of the BEC model is regular. The mass distribution is being a function of the radius and central density, decreases slowly with r in such a way that most of the matter concentrated in a core-like region. This theoretical behavior of the BEC model is in sharp contrast with the cuspy nature of the models arise from the numerical simulations [6].

On the other hand, the NFW density profile is singular(cusp) at the center of the galaxy ($\rho_{NFW}(r) \to \infty$ as $r \to 0$). It increases very rapidly for small r while for large radial distance, it tends more rapidly to zero than the BEC profile. The radius, $R_{\rm DM}$, for the dark matter halo in the BEC model is finite and it corresponds to a surface on which density tends to zero. But for the NFW density profile no such radius exists. Therefore, Bose-Einstein condensation processes in dwarf galaxies can remove the central cusps predicted by dark- matter- only cosmological simulations to convert it into a dark matter halo characterized by a large and almost constant density core consistent with normal dwarf galaxies in the local universe [18, 19].

The logarithmic slope of the density profile $\alpha(r)$ (defined by $\alpha(r) = \frac{d[\log(\rho_{DM})]}{d[\log(r)]}$) for

the BEC model is given by

$$\begin{aligned} \alpha(r) &= -[1 - \frac{r\pi}{R_{\rm DM}} \cot(r\pi/R_{\rm DM})] \\ &= -\frac{\pi^2 v_{tg}^2(r)}{4\pi G \rho_{DM} R_{\rm DM}^2}. \end{aligned} \tag{3.36}$$

As $r \to R_{\rm DM}$, $\alpha(r) \to \infty$. Observations of the rotational curves of dwarf galaxies [19] and low surface brightness galaxies [20], provide us the mean value of the logarithmic inner slopes of the mass density profiles which is defined by [22]

$$\langle \alpha_{in} \rangle = \frac{1}{R_{in}} \int_0^{R_{in}} \alpha(r) dr, \tag{3.37}$$

where R_{in} is the radius of the inner core of the dark matter distribution. For $R_{in} = 0.6R$, $\langle \alpha_{in} \rangle = -0.2818$ which is consistent with the limit -0.29 ± 0.07 obtained in [19]. Therefore, $\langle \alpha_{in} \rangle$ in the BEC dark matter model is in good concordance with the observations. Where as, in the CDM model $\alpha(r) \approx -1$.

The discrepancies of masses in standard estimation and BEC may open a new window to solve the mass discrepancy problem between observations and simulations [21]. The standard core-like models (e.g. pseudo-isothermal model) dominated by a central constant-density core [19], forecast a much higher galaxy mass than the BEC models. Since dwarf galaxies are supposed to highly fill with dark matter, the possibility of recovering their rotational curves and the mean value of the logarithmic inner slope of the mass density profiles, shows a significant instance in favour of the strongly-coupled dilute Bose-Einstein condensate dark matter model.

The density profile of the BEC model slowly decreases with r and have a large

core. All the physical quantities are regular in any of the physical parameters for all r. Therefore, they can be forecasted from the model and can be compared with the corresponding observational parameters. This offers a systematical comparison of the BEC model with other standard models or astrophysical observations.

3.6 A common behavior among some dark matter profiles

Observations suggest that the behavior of Pseudo Isothermal (PI) profile, Navarro-Frenk-White (NFW) profile and some Scalar Field Dark Matter (SFDM) profiles in the central region of galaxies are different. The density profile of NFW profile diverges at the centre of the halo while PI density profile is consistent with a constant density core. In this section, we will show that the tangential velocity($v_{tg}(r)$), the logarithmic slope of the density profile($\alpha(r)$) and the logarithmic slope of the rotational curve($\beta(r)$) of Pseudo Isothermal (PI) profile[23], Navarro-Frenk-White (NFW) profile and some other two dark matter profiles are nearly constant in the region far away from the centre of the galaxy.

Pseudo Isothermal (PI) profile

The density function for the Pseudo Isothermal (PI) profile (Begeman et al. 1991)

is given by [23]

$$\rho_{PI}(r) = \frac{\rho_0^{PI}}{1 + (r/R_c)^2}, \tag{3.38}$$

where R_c is the scale radius and ρ_0^{PI} is the central density of the dark matter.

The mass(m) within the radius r is given by [24]

$$m(r) = \int_0^r 4\pi\rho r^2 dr = 4\pi\rho_0^{PI}(rR_c^2 + ArcTan[\frac{R_c}{r}]R_c^3). \tag{3.39}$$

This gives the tangential velocity of a test particle at a distance r,

$$v_{tg}(r) = (\frac{Gm(r)}{r})^{1/2} = 2\sqrt{\pi}\sqrt{\frac{\rho_0^{PI}GR_c^2(r + ArcTan[\frac{R_c}{r}]R_c)}{r}}. \tag{3.40}$$

The logarithmic slope of the density profile is given by

$$\alpha(r) = \frac{d(\lg(\rho_{PI}))}{d(\lg(r))} = -\frac{2r^2}{r^2 + R_c^2}. \tag{3.41}$$

Similarly, the logarithmic slope of the rotational curves is given by

$$\beta(r) = \frac{d(\lg(v_{tg}))}{d(\lg(r))} = -\frac{R_c(r^2 ArcTan[\frac{R_c}{r}] + rR_c + ArcTan[\frac{R_c}{r}]R_c^2)}{2(r + ArcTan[\frac{R_c}{r}]R_c)(r^2 + R_c^2)}. \tag{3.42}$$

Navarro-Frenk-White (NFW) profile

The NFW profile emerges from numerical simulations that uses only CDM and is based on the CDM model (Dubinski et al. 1991; Navarro et al. 1996, 1997). The mass(m), tangential velocity($v_{tg}(r)$), the logarithmic slope of the density profile($\alpha(r)$), the logarithmic slope of the rotational curve($\beta(r)$) of the NFW density profile (3.28) are given by [24]

$$m(r) = 4\pi\rho_s r_s^3(Log[r + r_s] + \frac{r_s}{r + r_s}), \tag{3.43}$$

$$v_{tg}(r) = 2\sqrt{\pi}\sqrt{\frac{\rho_s r_s^3 G(Log[r+r_s] + \frac{r_s}{r+r_s})}{r}}, \tag{3.44}$$

$$\alpha(r) = -\frac{3r + r_s}{r + r_s}, \tag{3.45}$$

$$\beta(r) = -\frac{r^2(-1 + Log[r+r_s]) + (r + 2rLog[r+r_s])r_s + (1 + Log[r+r_s])r_s^2}{2(r+r_s)(rLog[r+r_s] + (1+Log[r+r_s])r_s)}. \tag{3.46}$$

Here, for the comparison, we have considered the following density profiles –

Case-I : $\rho = \frac{1}{8\pi}\frac{r^{-(4+l)}[D(l^3+l^2-4l-4)+l^2r^{2+l}]}{l^2-4}$ where D is an arbitrary constant of integration, $D \geq 10^{-7}$ and $l \sim 10^{-6}$ [25].

Case-II : $\rho = \frac{1}{8\pi}[\frac{l(l+2)r^{-2}}{\beta} + \frac{Dr^{-\alpha}l(l+1)}{l+4}]$ where $\alpha = \frac{l^2+4l+12}{l+4}$ and $\beta = l^2 + 2l + 4$ [26].

The mass($m(r)$), tangential velocity($v_{tg}(r)$), logarithmic slope of the density profile($\alpha(r)$) and logarithmic slope of the rotational curve($\beta(r)$) of the above profiles are given by [24] :

Case-I :

$$m(r) = \frac{l^2 r - D(-4+l^2)r^{(-1-l)}}{2(-4+l^2)}, \tag{3.47}$$

$$v_{tg}(r) = \frac{\sqrt{\frac{Gr^{-2-l}(-D(-4+l^2)+l^2r^{2+l})}{(-4+l^2)}}}{\sqrt{2}}, \tag{3.48}$$

$$\alpha(r) = -\frac{D(-16 - 20l + 5l^3 + l^4) + 2l^2r^{(2+l)}}{D(-4 - 4l + l^2 + l^3) + l^2r^{(2+l)}}, \tag{3.49}$$

$$\beta(r) = -\frac{D(-2+l)(2+l)^2}{2D(-4+l^2) - 2l^2r^{(2+l)}}. \tag{3.50}$$

Case-II :

$$m(r) = \frac{1}{2}(\frac{l(l+2)r}{4+2l+l^2} - Dr^{-\frac{l(l+1)}{4+l}}), \tag{3.51}$$

$$v_{tg}(r) = \frac{\sqrt{\frac{G(\frac{l(l+2)r}{4+2l+l^2} - Dr^{-\frac{l(l+1)}{4+l}})}{r}}}{\sqrt{2}}, \tag{3.52}$$

$$\alpha(r) = \frac{r(-\frac{2l(l+2)}{(4+2l+l^2)r^3} - \frac{Dl(l+1)(12+4l+l^2)r^{-\frac{16+5l+l^2}{4+l}}}{(4+l)^2})}{\frac{l(l+2)}{(4+2l+l^2)r^2} + \frac{Dl(l+1)r^{-\frac{12+4l+l^2}{4+l}}}{4+l}}, \tag{3.53}$$

$$\beta(r) = -\frac{D(4+2l+l^2)^2}{2(4+l)(D(4+2l+l^2) - l(2+l)r^{1+\frac{l(l+1)}{4+l}})}. \tag{3.54}$$

Now, we will plot the graph of the tangential velocity($v_{tg}(r)$), logarithmic slope of the density profile($\alpha(r)$) and logarithmic slope of the rotational curve($\beta(r)$) for PI profile, NFW profile, Case-I and Case-II for the galaxy ESO1870510 [23] with $D = 10^{-2}$. Now the graphs are as follows [24] **:**

For PI profile :

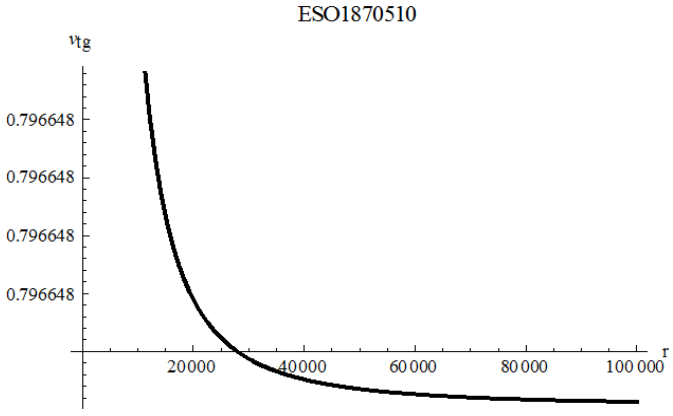

Figure 3.1. Plot of $v_{tg}(r)$ vs r for the galaxy ESO1870510 (for PI profile).

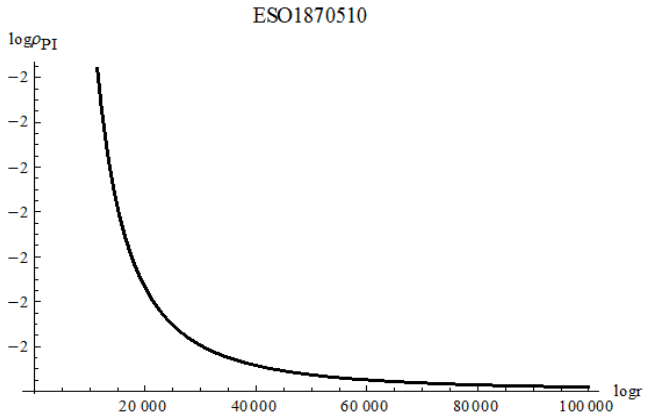

Figure 3.2. Plot of $\alpha(r)$ vs r for the galaxy ESO1870510 (for PI profile).

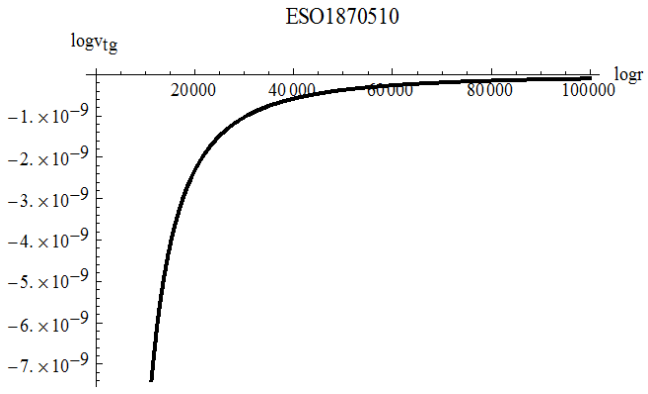

Figure 3.3. Plot of $\beta(r)$ vs r for the galaxy ESO1870510 (for PI profile).

For NFW profile :

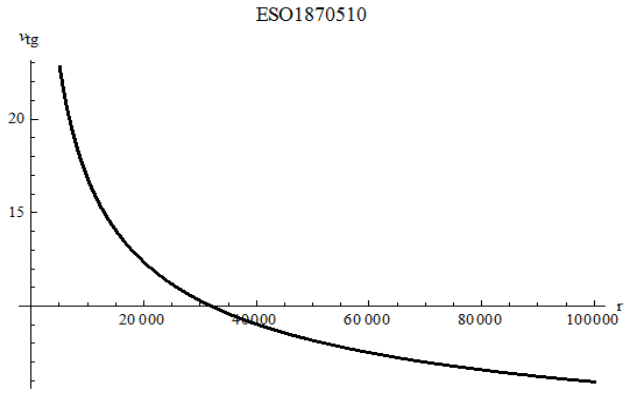

Figure 3.4. Plot of $v_{tg}(r)$ vs r for the galaxy ESO1870510 (for NFW profile).

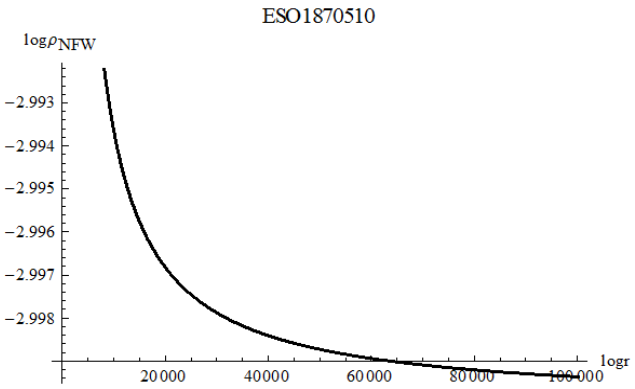

Figure 3.5. Plot of $\alpha(r)$ vs r for the galaxy ESO1870510 (for NFW profile).

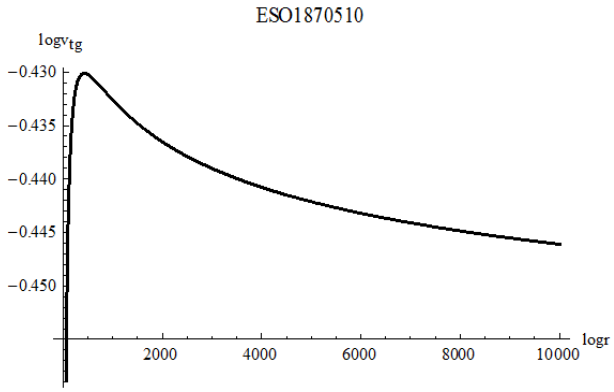

Figure 3.6. Plot of $\beta(r)$ vs r for the galaxy ESO1870510 (for NFW profile).

For Case-I with $D = 10^{-2}$:

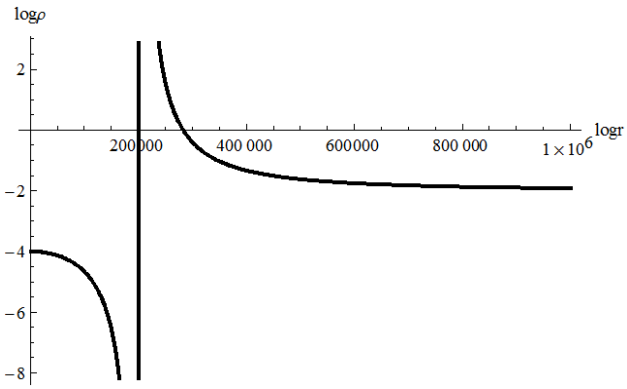

Figure 3.7. Plot of $\alpha(r)$ vs r for Case-I with $D = 10^{-2}$ and $l = 10^{-6}$.

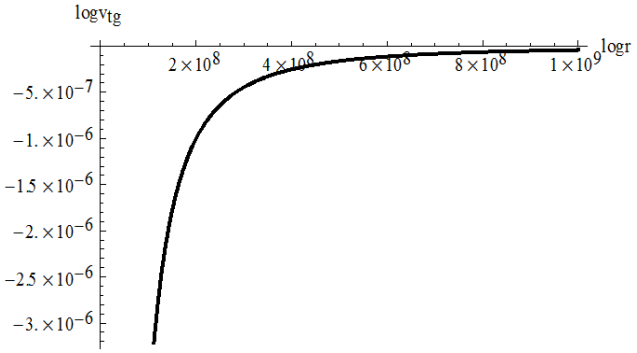

Figure 3.8. Plot of $\beta(r)$ vs r for Case-I with $D = 10^{-2}$ and $l = 10^{-6}$.

For Case-II with $D = 10^{-2}$:

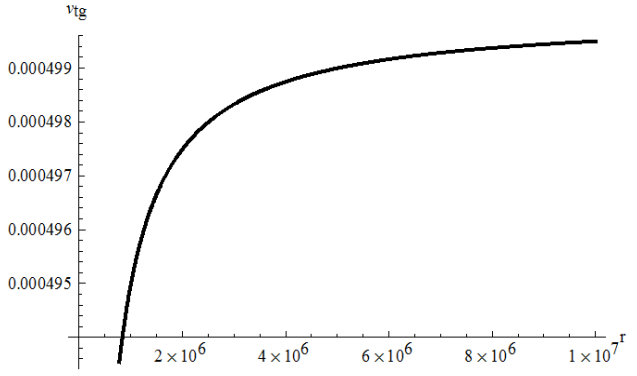

Figure 3.9. Plot of $v_{tg}(r)$ vs r for Case-II with $D = 10^{-2}$ and $l = 10^{-6}$.

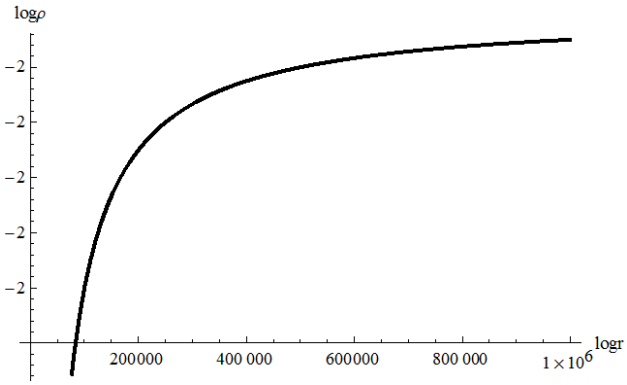

Figure 3.10. Plot of $\alpha(r)$ vs r for Case-II with $D = 10^{-2}$ and $l = 10^{-6}$.

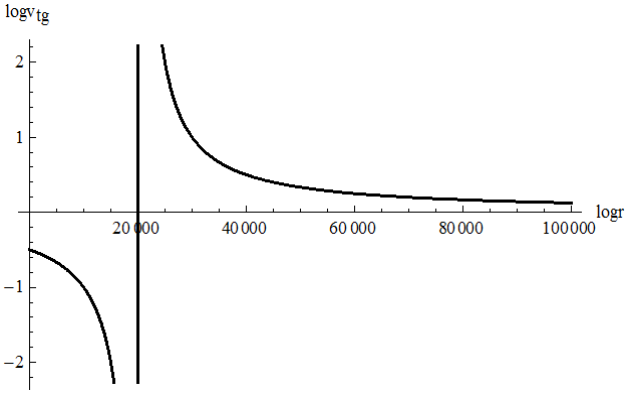

Figure 3.11. Plot of $\beta(r)$ vs r for Case-II with $D = 10^{-2}$ and $l = 10^{-6}$.

The above profiles emerge from different points of view with different postulations. The NFW profile emerges from numerical simulations that use only CDM and are based on the CDM model (Dubinski et al. 1991; Navarro et al. 1996, 1997). We, generally, use the PI profiles to describe the constant density behavior in these galaxies. The above profiles may have different behavior in the central region but the plotted graphs suggest that in the large distance scale the tangential velocity ($v_{tg}(r)$), the logarithmic slope of the density profile($\alpha(r)$) and the logarithmic slope of the rotational curve($\beta(r)$) give a constant value i.e. the tangential velocity and density are nearly constant in the region far away from the centre of the galaxies. Similar results can be found for other values of $D(\geq 10^{-7})$ up to a wide range of large values of D and for the other galaxies in [23].

Again, $D \geq 10^{-7}$ is the condition that must be maintained in order to have a non-Newtonian halo. So for a non-Newtonian halo, the tangential velocity and density are nearly constant for large values of r. But we think that, it is necessary to use the observations in order to make same conclusions for other halo models.

References

[1] F. Dalfovo, S. Giorgini, L. P. Pitaevskii and S. Stringari, Rev. Mod. Phys. **71**, 463 (1999); E. A. Cornell and C. E. Wieman, Rev. Mod. Phys. **74**, 875 (2002); W. Ketterle, Rev. Mod. Phys. **74**, 1131 (2002); L. Pitaevskii and S. Stringari, Bose-Einstein condensation, Clarendon Press, Oxford (2003); R. A. Duine and H. T. C. Stoof, Phys. Repts. **396**, 115 (2004).

[2] C. J. Pethick and H. Smith, Bose-Einstein condensation in dilute gases, Cambridge, Cambridge University Press, (2008).

[3] P.-H. Chavanis, Phys. Rev. D **84**, 043531 (2011).

[4] P.-H. Chavanis and L. Delfini, Phys. Rev. D **84**, 043532 (2011).

[5] W. Hu, R. Barkana and A. Gruzinov, Phys. Rev. Lett. **85**, 1158 (2000).

[6] J.F. Navarro, C.S. Frenk and S.D.M. White, ApJ, **462**, 563, (1996); J.F. Navarro, C.S. Frenk and S.D.M. White, ApJ, **490**, 493, (1997).

[7] B. Moore et al, MNRAS, **310**, 1147, (1999); S. Ghigna et al, astro-ph/9910166.

[8] E.L. Lokas and G. Mamon, MNRAS, **321**, 155, (2001).

[9] C. G. Bohmer and T. Harko, JCAP **06**, 025 (2007).

[10] S. Chandrasekhar, An introduction to the study of stellar structure, Dover Publications, New York (1957).

[11] P. H. Chavanis, T. Harko, Phys. Rev. D **86**, 064011 (2012).

[12] N. K. Glendenning, Compact Stars, Nuclear Physics, Particle Physics and General Relativity, Springer, New York (2000).

[13] D. Boyanovsky, H. J. de Vega, and N. Sanchez, Phys. Rev. D **77**, 043518 (2008)

[14] V. R. Eke, J.F. Navarro and M. Steinmetz, Ap J, **554**, 114, (2001). See also V. Avila–Rees et al, AA, **412**, 633, (2003).

[15] E.L. Lokas and Y. Hoffman, astro-ph/0108283; E.L. Lokas Acta Phys.Polon., B**32**, 3643-3654, (2001).

[16] Tonatiuh Matos, Darıo Nunez and Roberto A Sussman, arXiv: astro-ph/0410215v1 7 Oct 2004.

[17] A. Burkert, Astrophys. J. Letters **447**, L25 (1995).

[18] F. Walter, E. Brinks, W. J. G. de Blok, F. Bigiel, R. C. Kennicutt, M. Thornley, and A. Leroy, Astron. J. **136**, 2563 (2008).

[19] S.-H. Oh, W. J. G. de Blok, E. Brinks, F. Walter, and R. C. Kennicutt, Jr., arXiv:1011.0899 (2010).

[20] W. J. G. de Blok, S. S. McGaugh, A. Bosma and V. C. Rubin, Astrophys. J. **552**, 23 (2001)

[21] T. Sawala, Q. Guo, C. Scannapieco, A. Jenkins and S. White, arXiv: 1003.0671 (2010).

[22] T. Harko, JCAP 1105, 022 (2011).

[23] Victor H. Robles and T. Matos, MNRAS, **422**, 282-289, 2012.

[24] Kamal K. Nandi, Mithun Ghosh, Vestnik BSPU, **21**, 63 (2013).

[25] Kamal Nandi et al., Phys.Rev. D **80,** 047301, 2009.

[26] F. Rahaman et al., Mon.Not.Roy.Astron.Soc.**399,** 2079-2087, 2009.